HHS Public Access

Author manuscript

ACS Sens. Author manuscript; available in PMC 2024 February 05.

Published in final edited form as:

ACS Sens. 2023 November 24; 8(11): 4008–4013. doi:10.1021/acssensors.3c00717.

Detection of Pulmonary Fibrosis with a Collagen-Mimetic Peptide

Isabella M. Borgula[†], **Sergey Shuvaev**[#,‡], **Eric Abston**[‡,§], **Nicholas J. Rotile**[‡], **Jonah Weigand-Whittier**[‡], **Iris Y. Zhou**[‡], **Peter Caravan**[#,‡,*], **Ronald T. Raines**[†,*]

[†]Department of Chemistry, Massachusetts Institute of Technology, Cambridge, Massachusetts 02139, United States

[#]Department of Radiology, Massachusetts General Hospital, Boston, Massachusetts 02124, United States

[‡]Athinoula A. Martinos Center for Biomedical Imaging, The Institute for Innovation in Imaging, Massachusetts General Hospital and Harvard Medical School, 149 Thirteenth Street, Charlestown, Massachusetts 02129, United States

[§]Department of Thoracic Surgery, Massachusetts General Hospital, Boston, Massachusetts 02124, United States

Abstract

Idiopathic pulmonary fibrosis (IPF) is a disease of unknown etiology that is characterized by excessive deposition and abnormal remodeling of collagen. IPF has a mean survival time of only 2–5 years from diagnosis, creating a need to detect IPF at an earlier stage when treatments might be more effective. We sought to develop a minimally invasive probe that could detect molecular changes in IPF-associated collagen. Here, we describe the design, synthesis, and performance of [^{68}Ga]Ga·DOTA–CMP, which comprises a positron-emitting radioisotope linked to a collagen-mimetic peptide (CMP). This peptide mimics the natural structure of collagen and detects irregular collagen matrices by annealing to damaged collagen triple helices. We assessed the ability of the peptide to detect aberrant lung collagen selectively in a bleomycin-induced mouse model

[*]**Corresponding Authors Peter Caravan** – *Department of Radiology, Massachusetts General Hospital, Boston, Massachusetts 02124, United States; Athinoula A. Martinos Center for Biomedical Imaging, The Institute for Innovation in Imaging, Massachusetts General Hospital and Harvard Medical School, 149 Thirteenth Street, Charlestown, Massachusetts 02129, United States;* pcaravan@mgh.harvard.edu; **Ronald T. Raines** – *Department of Chemistry, Massachusetts Institute of Technology, Cambridge, Massachusetts 02139, United States;* rtraines@mit.edu.

Isabella M. Borgula – *Department of Chemistry, Massachusetts Institute of Technology, Cambridge, Massachusetts 02139, United States*

Sergey Shuvaev – *Department of Radiology, Massachusetts General Hospital, Boston, Massachusetts 02124, United States; Athinoula A. Martinos Center for Biomedical Imaging, The Institute for Innovation in Imaging, Massachusetts General Hospital and Harvard Medical School, 149 Thirteenth Street, Charlestown, Massachusetts 02129, United States*

Eric Abston – *Department of Thoracic Surgery, Massachusetts General Hospital, Boston, Massachusetts 02124, United States*

Nicholas J. Rotile – *Athinoula A. Martinos Center for Biomedical Imaging, The Institute for Innovation in Imaging, Massachusetts General Hospital and Harvard Medical School, 149 Thirteenth Street, Charlestown, Massachusetts 02129, United States*

Jonah Wiegand-Whittier – *Athinoula A. Martinos Center for Biomedical Imaging, The Institute for Innovation in Imaging, Massachusetts General Hospital and Harvard Medical School, 149 Thirteenth Street, Charlestown, Massachusetts 02129, United States*

Iris Y. Zhou –*Athinoula A. Martinos Center for Biomedical Imaging, The Institute for Innovation in Imaging, Massachusetts General Hospital and Harvard Medical School, 149 Thirteenth Street, Charlestown, Massachusetts 02129, United States*

The authors declare no competing financial interest.

of pulmonary fibrosis using positron emission tomography (PET). [^{68}Ga]Ga·DOTA–CMP PET demonstrated higher and selective uptake in a fibrotic mouse lung compared to controls, minimal background signal in adjacent organs, and rapid clearance via the renal system. These studies suggest that [^{68}Ga]Ga·DOTA–CMP identifies fibrotic lungs and could be useful in the early diagnosis of IPF.

Graphical Abstract

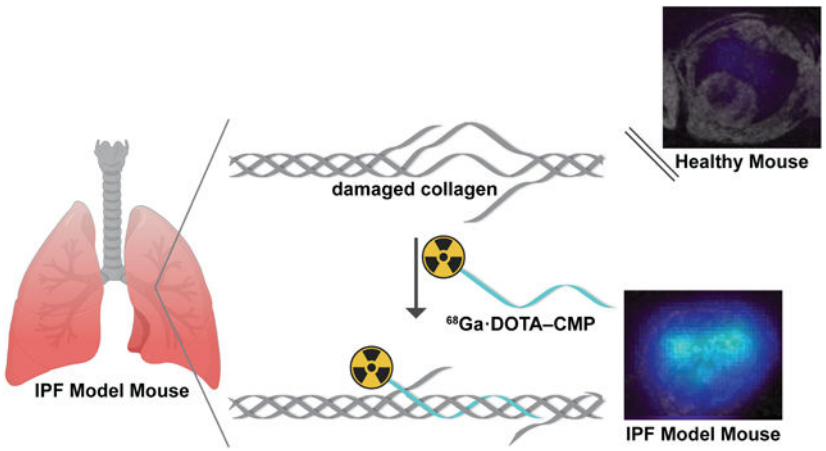

Keywords

extracellular matrix; fluoroproline; idiopathic pulmonary fibrosis; imaging; lung; positron emission tomography; triple helix; probe

Collagen is the most abundant protein in the human body.[1] This abundance avails the extraordinary stability conferred by its hierarchical structure. Collagen is a right-handed triple helix consisting of three left-handed polyproline type-II (PPII) helices.[1,2] Its amino acid sequence has a repeating triplet, XaaYaaGly, where Xaa is most commonly (*2S*)-proline (Pro) and Yaa is most commonly (2*S*,4*R*)-4-hydroxyproline (Hyp).[3] The high abundance of Pro and Hyp residues preorganize collagen strands for helix formation, whereas the small glycine (Gly) residue fits into the core of the triple helix.[4]

In healthy tissue, collagen helices undergo extensive proteolytic remodeling for tissue maintenance.[5] When these processes are dysregulated, excessive levels of proteolysis-destabilized collagen triple helices are produced that can denature at biological temperature.[6] This damaged collagen can be targeted with collagen-mimetic peptides (CMPs), which mimic the natural structure of collagen and can anneal to dissociated collagen (Figure 1).[7,8] Thus, CMPs can anchor pendant molecules to tissues with damaged or abnormal collagen.[8-11]

The extracellular matrix is damaged or abnormal in a variety of fibroproliferative diseases. For example, pulmonary fibrosis, which is a pathology associated with a range of lung diseases, is characterized by dysregulated matrix metalloproteinase production.[12] Idiopathic

pulmonary fibrosis (IPF) is the prototypic form of pulmonary fibrosis and is associated with particularly severe symptoms.[13]

We reasoned that CMPs could be noninvasive probes for detecting pulmonary fibrosis. We anticipated two possible means by which collagen could lose integrity. First, rapid collagen production and abnormal collagen remodeling in IPF lungs could lead to an incorrectly remodeled collagen matrix. During fibrosis, collagen triple helices might not be adequately interdigitated for fibril formation, yielding less stable triple helices that are more likely to possess dissociated domains where CMPs can anneal.[14] This modality is supported by the correlation of an IPF phenotype with diminished collagen ordering within a tissue.[15] Tropocollagen triple helices have lower thermostability than do helices incorporated into higher-order structures and are unstable at 37 °C,[6,14] thus increasing the propensity for IPF triple helices to denature in a mammal and provide binding sites for CMPs. Second, matrix-metalloproteinases are upregulated in active pulmonary fibrosis and in the corresponding mouse model.[16] These enzymes cleave strands in collagen triple helices, again providing binding sites for CMPs.[12]

The current paradigm for IPF diagnosis is high-resolution computed tomography (HRCT). The median survival of IPF ranges from 2–5 years from diagnosis,[17] emphasizing the need for early detection of IPF when treatments might be more effective. Clinical trial data with two approved antifibrotic therapies showed a benefit in patients with more preserved lung function and imply greater benefit if disease could be treated earlier, which would require early detection.[18,19] We sought to leverage positron emission tomography (PET) to achieve this goal, as this modality is known for its high sensitivity and ability to detect molecular markers. Developing a collagen-specific PET tracer could serve as a complementary tool to conventional HRCT. For example PET could be valuable in the early detection of IPF, especially in patients at high risk for the disease, such as those with a family history of IPF[20] or interstitial lung abnormalities.[21] Moreover, in cases where HRCT cannot distinguish between fibrosis and nonfibrotic inflammation, a biopsy is required to identify signs of fibrosis histologically.[22] Unfortunately, biopsy carries risks of morbidity and mortality and only samples a tiny fraction of the lung.[23] The direct visualization of damaged collagen as a molecular signature of fibrosis has the potential to identify fibrosis throughout the entire lung. Other collagen-targeted PET probes have been developed for minimally invasive pulmonary fibrosis detection;[14,24-26] however, these probes generally bind to intact rather than damaged collagen.

We sought to enhance existing IPF diagnostic techniques by designing a novel, minimally invasive probe to detect molecular changes in IPF-associated collagen. Design criteria led us to [^{68}Ga]Ga·DOTA–CMP, which is detectable by PET/MR, an imaging modality that delivers a lower radiation dose than PET/CT while supplying multifaceted MR details on soft tissue anatomy. [^{68}Ga]Ga·DOTA–CMP contains the peptide (Gly-Ser)$_2$-Gly-(flp-Hyp-Gly)$_7$, where flp refers to (2*S*,4*S*)-4-fluoroproline. This peptide can anneal to damaged collagen triple helices (Figure 2A).[8,27] Importantly, this peptide resists homotrimer formation, a process that competes deleteriously with forming a triple helix with damaged collagen.[8,27,28] That resistance is due to a steric clash between a 4*S*-substituted and a 4*R*-substituted proline residue in each register of a triple helix.[29,30] The nonnatural residue

flp differs from the natural residue Pro only by the replacement of a single H atom with F, and the H-flp-OH amino acid is not toxic to human cells.[8]

As a control, we synthesized a compositional isomer (CI), [^{68}Ga]Ga·DOTA–CI, which contains the peptide (Gly-Ser)$_2$-Gly-(Hyp-flp-Gly)$_7$ (Figure 2B). The Hyp⟷flp sequence permutation interferes with the stereochemical requirements for forming a collagen helix.[31,32] Accordingly, this peptide cannot anneal to damaged collagen, despite its amino acid composition.[8]

The N-terminal Gly-Ser-Gly-Ser-Gly sequence serves as a flexible, hydrophilic linker for conjugation to the radioisotope chelator, 1,4,7,10-tetraazacyclododecane-1,4,7,10-tetraacetic acid (DOTA). We selected DOTA because of the high stability of its complex with ^{68}Ga, a positron-emitting radioisotope that does not require a cyclotron for generation.[33,34] ^{68}Ga has a half-life of 68 min, providing an ideal half-life for PET imaging while requiring a dose that is low enough to mitigate total radiation exposure.[35] This isotope decays into ^{68}Zn, which is an essential trace element.[36] ^{68}Ga has been widely applied in the clinical community for PET, facilitating clinical translation.[37,38]

The two peptides were synthesized via automated microwave-assisted Fmoc-mediated solid-phase peptide synthesis (Scheme S1) and purified by reversed-phase high-performance liquid chromatography (RP-HPLC). The purified peptides were conjugated to NHS-ester-activated DOTA at the N-terminus. Following conjugation, the DOTA–peptide conjugates were purified by preparative RP-HPLC. Their purities were verified with analytical RP-HPLC (Figure S1) and matrix-assisted laser desorption/ionization–time-of-flight mass spectrometry (Figure S2).

The structure of DOTA–CMP was assessed by circular dichroism (CD) spectroscopy. A solution of DOTA–CMP displayed a shallow peak at 225 nm and no cooperative denaturation with an increasing temperature (Figure S3). These data are consistent with signatures of PPII structures that do not form triple helices and confirm that DOTA–CMP remains to collagen strands, we recorded CD spectra of a 1:1 mixture of DOTA–CMP and (ProProGly)$_7$. (ProProGly)$_7$ was used as a proxy for damaged collagen because it bears the canonical XaaYaaGly motif but is too short to form a homotrimer, avoiding a confounding CD signal in the mixture.[8,29] Additionally, (ProProGly)$_7$ does not have a 4*R*-substituted proline residue, thereby avoiding steric clashes with the flp residues of DOTA–CMP.[29] The CD spectra of the 1:1 mixture of DOTA–CMP:(ProProGly)$_7$ exhibited a strong peak at 225 nm, cooperative denaturation with increasing temperature, and a T_m value of 34 °C (Figure S3). These data suggest that the addition of DOTA to the N terminus of the CMP did not impede its ability to form heterotrimers with collagen.

Our strategy relies on the CMP being stable in sera and plasma. We assessed this stability in two ways. First, we incubated 5(6)-TAMRA–(Gly-Ser)$_2$-Gly-(flp-Hyp-Gly)$_7$-NH$_2$ in sera. During a 48-h time course, we detected no degradation in human serum and only slight degradation in mouse serum (Figure S4). Then, we radiolabeled DOTA–CMP with ^{64}Cu by adapting a known procedure.[39] (The 12.7 h half-life of ^{64}Cu provides a longer time course for this analysis than does ^{68}Ga.) We observed no degradation or proteolysis

of ^{64}Cu·DOTA–CMP over 21 h in human plasma, as analyzed with instant thin-layer chromatography (Figure S5). This high stability in serum and plasma is consistent with that of other CMPs.[40]

Next, we radiolabeled DOTA–CMP and DOTA–CI with ^{68}Ga,[39] giving the desired product with ≥90% radiochemical yield as determined by radio-HPLC (Figure S6). We assessed the ability of the two ^{68}Ga-labeled conjugates to detect IPF in vivo by using a validated mouse model of IPF.[41,42] To create the model, we injured male C57BL/6 mice with a single transtracheal instillation of bleomycin in phosphate-buffered saline (PBS) (Figure S7A).[14] Fourteen days later, the mice developed pulmonary fibrosis, which was confirmed by histopathological analyses. Those analyses revealed excessive interstitial deposition of collagen as demonstrated by staining collagen with Picrosirius red as well as the destruction of lung architecture (Figure S8).[14,42] As a control, sham animals, which received transtracheally administered PBS, were healthy and showed no signs of pulmonary disease (Figure S6), in line with previously reported results.[14] Mice were injected in their tail vein with [^{68}Ga]Ga·DOTA–CMP or [^{68}Ga]Ga·DOTA–CI (50–150 μCi) and imaged with 4.7 T PET/MR. After imaging, the mice were sacrificed for ex vivo analysis 90 min after administration of the probes. PET imaging showed that [^{68}Ga]Ga·DOTA–CMP was not retained in the lungs of sham mice and displayed a nearly undetectable signal in all satellite organs (Figure 3). Background signal was observed in the kidneys and bladder, which are involved in renal excretion of the probe following its rapid elimination from the blood (estimated $t_{1/2}$ = 6.3 min). In comparison to sham mice, [^{68}Ga]Ga·DOTA–CMP was taken up in the lungs of IPF mouse models (Figures 3, S9, and S10). Comparable biodistribution was observed in satellite organs. In vivo quantification of the decay-corrected PET signal in the lungs averaged over 50–60 min revealed that [^{68}Ga]Ga·DOTA–CMP had a 4.9-fold higher lung uptake in IPF mouse models than sham mice, $P < 0.001$ (Figure 4A). Additionally, the ratio of specific uptake in the right lung to nonspecific uptake in muscle (RLMR) was compared in sham and bleomycin-injured mice injected with [^{68}Ga]Ga·DOTA–CMP. The RLMR was also found to be 2.6-fold higher for bleomycin-injured mice compared to sham mice (Figure 4B). Following imaging, mice were sacrificed and dissected, and the uptake of probe in individual excised organs was quantified with a gamma counter. Minimal background signal was observed in satellite organs, excluding those required for expected renal excretion (Figure S11).

To examine the specificity of [^{68}Ga]Ga·DOTA–CMP further, we performed a paired study of mice injected with both [^{68}Ga]Ga·DOTA–CMP and the control probe, [^{68}Ga]Ga·DOTA–CI (Figure S7B). For this study, mice were injected with [^{68}Ga]Ga·DOTA–CMP and imaged. After 24 h, ^{68}Ga had decayed to background levels, and the same mice were injected with [^{68}Ga]Ga·DOTA–CI and imaged. As with [^{68}Ga]Ga·DOTA–CMP in sham mice, the control peptide [^{68}Ga]Ga·DOTA–CI was not taken up in the lungs of IPF mouse models. In vivo quantification of the decay-corrected PET signal in the lungs averaged over 50–60 min revealed that [^{68}Ga]Ga·DOTA–CMP had a significantly (3.6-fold) higher lung uptake in IPF mouse models compared to [^{68}Ga]Ga·DOTA–CI in the same mouse model (Figure 4C). We also found that [^{68}Ga]Ga·DOTA–CMP had a significantly (1.7-fold) higher RLMR, supporting the selectivity of CMPs for collagen in lungs afflicted with bleomycin-induced pulmonary fibrosis (Figure 4D).

To further support the selectivity of our peptide for pulmonary fibrotic tissue and not other organs, we integrated the in vivo PET signal of the kidneys over the time of the study, that is, from 0 to 60 min after injection into bleomycin-injured mice that had been treated with [^{68}Ga]Ga·DOTA–CMP and [^{68}Ga]Ga·DOTA–CI on consecutive days (Figure S7B). We did not observe a significant difference in organ retention (P = 0.0878; Figure S12), suggesting that the higher kidney PET signal in the bleomycin-injured animal in Figure 3 compared to the sham mouse is simply due to slower renal clearance in the sick mouse and is not an effect of [^{68}Ga]Ga·DOTA–CMP binding selectively to a target in the kidneys of mice with localized lung injury.

To better reflect the trends observed in tissues, we compared the total ex vivo probe uptake in each lung (Figure 4E). Sham mice injected with [^{68}Ga]Ga·DOTA–CMP and IPF mouse models injected with [^{68}Ga]Ga·DOTA–CI did not differ significantly in probe uptake and biodistribution. This resemblance suggests that the lung enrichment observed in bleomycin-injured mice treated with the CMP was due to CMP binding, rather than a general lag in the clearance of the probe. In contrast, the lung uptake of [^{68}Ga]Ga·DOTA–CMP was 11- to 12-fold higher in IPF mouse models than sham mice and 3-fold higher than the uptake of [^{68}Ga]Ga·DOTA–CI in IPF mouse models.

Finally, we estimated the mass of collagen in the excised mouse lungs by quantifying Hyp, which is a common residue in collagen but not other proteins.[43] We then compared the mass of H-Hyp-OH found in each lung to the ex vivo lung uptake of [^{68}Ga]Ga·DOTA–CMP. We found that the uptake of [^{68}Ga]Ga·DOTA–CMP had little correlation with the lung Hyp content (R^2 = 0.33) (Figure S13), suggesting that this probe did not merely bind to overexpressed collagen in bleomycin-injured mice. These data are consistent with the binding of [^{68}Ga]Ga·DOTA–CMP to a specific biomarker of pulmonary fibrosis—damaged collagen triple helices (Figure 1).

In conclusion, we described the first use of CMPs as an in vivo probe for detecting pulmonary fibrosis. We find that CMPs report on molecular-level defects in disease-associated collagen, specifically, the presence of non-triple-helical collagen in a fibrotic lung. [^{68}Ga]Ga·DOTA–CMP displays specificity and strong uptake in the lungs of a bleomycin-injured IPF mouse model, resulting in up to 11-fold higher uptake in an IPF mouse model compared to controls. The unique mode-of-action of CMPs enables the detection of abnormal collagen production and remodeling, such as those found in pulmonary fibrosis. The specificity of [^{68}Ga]Ga·DOTA–CMP in vivo and its ability to selectively detect IPF make CMPs promising candidates for the diagnosis of other fibrotic diseases.

Supplementary Material

Refer to Web version on PubMed Central for supplementary material.

ACKNOWLEDGMENTS

We thank Dr. Jesús M. Dones, Jinyi Yang, and Yana D. Petri for conversations on peptide synthesis, Alana W. Ross and Matthew Drummond for assistance with animal handling and tissue collection, and Dr. Mariane Le Fur and Dr. Hua Ma for advice on radiolabeling. The TOC graphic was created with software from BioRender.com.

Funding

This work was supported by Grants R56 AR044276, R35 GM148220, R01 HL153606, R33 HL154125, S10 OD023503, S10 OD025234, S10 OD028499, and S10 OD032138 (NIH).

REFERENCES

(1). Shoulders MD; Raines RT Collagen structure and stability. Annu. Rev. Biochem 2009, 78, 929–958. [PubMed: 19344236]

(2). Okuyama K; Hongo C; Fukushima R; Wu G; Narita H; Noguchi K; Tanaka Y; Nishino N Crystal structures of collagen model peptides with Pro-Hyp-Gly repeating sequence at 1.26 Å resolution: Implications for proline ring puckering. Pept. Sci 2004, 76, 367–377.

(3). Ramshaw JAM; Shah NK; Brodsky B Gly-X-Y tripeptide frequencies in collagen: a context for host–guest triple-helical peptides. J. Struct. Biol 1998, 122, 86–91. [PubMed: 9724608]

(4). Cram DJ The design of molecular hosts, guests, and their complexes. Science 1988, 240, 760–767. [PubMed: 3283937]

(5). Page-McCaw A; Ewald AJ; Werb Z Matrix metalloproteinases and the regulation of tissue remodelling. Nat. Rev. Mol. Cell Biol 2007, 8, 221–233. [PubMed: 17318226]

(6). Leikina E; Mertts MV; Kuznetsova N; Leikin S Type I collagen is thermally unstable at body temperature. Proc. Natl. Acad. Sci. U. S. A 2002, 99, 1314–1318. [PubMed: 11805290]

(7). Chattopadhyay S; Murphy CJ; McAnulty JF; Raines RT Peptides that anneal to natural collagen in vitro and ex vivo. Org. Biomol. Chem 2012, 10, 5892–5897. [PubMed: 22522497]

(8). Dones JM; Tanrikulu IC; Chacko JV; Schroeder AB; Hoang TT; Gibson ALF; Eliceiri KW; Raines RT Optimization of interstrand interactions enables burn detection with a collagen-mimetic peptide. Org. Biomol. Chem 2019, 17, 9906–9912. [PubMed: 31720665]

(9). Chattopadhyay S; Guthrie KM; Teixeira L; Murphy CJ; Dubielzig RR; McAnulty JF; Raines RT Anchoring a cytoactive factor in a wound bed promotes healing. J. Tissue Eng. Regen. Med 2016, 10, 1012–1020. [PubMed: 24677775]

(10). Hwang J; Huang Y; Burwell TJ; Peterson NC; Connor J; Weiss SJ; Yu SM; Li Y In situ imaging of tissue remodeling with collagen hybridizing peptides. ACS Nano 2017, 11, 9825–9835. [PubMed: 28877431]

(11). Aronoff MR; Hiebert P; Hentzen NB; Werner S; Wennemers H Imaging and targeting LOX-mediated tissue remodeling with a reactive collagen peptide. Nat. Chem. Biol 2021, 17, 865–871. [PubMed: 34253910]

(12). Craig VJ; Zhang L; Hagood JS; Owen CA Matrix metalloproteinases as therapeutic targets for idiopathic pulmonary fibrosis. Am. J. Respir. Cell Mol. Biol 2015, 53, 585–600. [PubMed: 26121236]

(13). Désogère P; Montesi SB; Caravan P Molecular probes for imaging fibrosis and fibrogenesis. Chem. Eur. J 2019, 25, 1128–1141. [PubMed: 30014529]

(14). Désogère P; Tapias LF; Rietz TA; Rotile N; Blasi F; Day H; Elliott J; Fuchs BC; Lanuti M; Caravan P Optimization of a collagen-targeted PET probe for molecular imaging of pulmonary fibrosis. J. Nucl. Med 2017, 58, 1991–1996. [PubMed: 28611243]

(15). James DS; Jambor AN; Chang H-Y; Alden Z; Tilbury KB; Sandbo NK; Campagnola PJ Probing ECM remodeling in idiopathic pulmonary fibrosis via second harmonic generation microscopy analysis of macro/supramolecular collagen structure. J. Biomed. Opt 2020, 25, 014505.

(16). Kim JY; Choeng HC; Ahn C; Cho S-H Early and late changes of MMP-2 and MMP-9 in bleomycin-induced pulmonary fibrosis. Yonsei Med. J 2009, 50, 68–77. [PubMed: 19259351]

(17). Nathan SD; Shlobin OA; Weir N; Ahmad S; Kaldjob JM; Battle E; Sheridan MJ; du Bois RM Long-term course and prognosis of idiopathic pulmonary fibrosis in the new millennium. Chest 2011, 140, 221. [PubMed: 21729893]

(18). Albera C; Costabel U; Fagan EA; Glassberg MK; Gorina E; Lancaster L; Lederer DJ; Nathan SD; Spirig D; Swigris JJ Efficacy of pirfenidone in patients with idiopathic pulmonary fibrosis with more preserved lung function. Eur. Respir. J 2016, 48, 843–851. [PubMed: 27471208]

(19). Kolb M; Richeldi L; Behr J; Maher TM; Tang W; Stowasser S; Hallmann C; du Bois RM Nintedanib in patients with idiopathic pulmonary fibrosis and preserved lung volume. Thorax 2017, 72, 340–346. [PubMed: 27672117]

(20). Steele MP; Peljto AL; Mathal SK; Humphries S; Bang TJ; Oh A; Teague S; Cicchetti G; Sigakis C; Kropski JA; Loyd JE; Blackwell TS; Brown KK; Schwarz MI; Warren RA; Powers J; Walts AD; Markin C; Fingerlin TE; Yang IV; Lynch DA; Lee JS; Schwartz DA Incidence and progression of fibrotic lung disease in an at-risk cohort. Am. J. Respir. Crit. Care Med 2023, 207, 587–593. [PubMed: 36094461]

(21). Hoffman TW; van Es HW; Biesma DH; Grutters JC Potential interstitial lung abnormalities on chest X-rays prior to symptoms of idiopathic pulmonary fibrosis. BMC Pulm. Med 2022, 22, 329. [PubMed: 36038862]

(22). Lynch DA; Sverzellati N; Travis WD; Brown KK; Colby TV; Galvin JR; Goldin JG; Hansell DM; Inoue Y; Johkoh T; Nicholson AG; Knight SL; Raoof S; Richeldi L; Ryerson CJ; Ryu JH; Wells AU Diagnostic criteria for idiopathic pulmonary fibrosis: A Fleischner Society White Paper. Lancet Respir. Med 2018, 6, 138–153. [PubMed: 29154106]

(23). Hutchinson JP; Fogarty AW; McKeever TM; Hubbard RB In-hospital mortality after surgical lung biopsy for interstitial lung disease in the United States. 2000 to 2011. Am. J. Respir. Crit. Care Med 2016, 193, 1161–1167. [PubMed: 26646481]

(24). Désogère P; Tapias LF; Hariri LP; Rotile NJ; Rietz TA; Probst CK; Blasi F; Day H; Mino-Kenudson M; Weinreb P; Violette SM; Fuchs BC; Tager AM; Lanuti M; Caravan P Type I collagen-targeted PET probe for pulmonary fibrosis detection and staging in preclinical models. Sci. Transl. Med 2017, 9, eaaf4696. [PubMed: 28381537]

(25). Wahsner J; Désogère P; Abston E; Graham-O'Regan KA; Wang J; Rotile NJ; Schirmer MD; Santos Ferreira DD; Sui J; Fuchs BC; Lanuti M; Caravan P ^{68}Ga–NODAGA–indole: An allysine-reactive positron emission tomography probe for molecular imaging of pulmonary fibrogenesis. J. Am. Chem. Soc 2019, 141, 5593–5596. [PubMed: 30908032]

(26). Jailkhani N; Ingram JR; Rashidian M; Rickelt S; Tian C; Mak H; Jiang Z; Ploegh HL; Hynes RO Noninvasive imaging of tumor progression, metastasis, and fibrosis using a nanobody targeting the extracellular matrix. Proc. Natl. Acad. Sci. U. S. A 2019, 116, 14181–14190. [PubMed: 31068469]

(27). Bennink LL; Li Y; Kim B; Shin IJ; San BH; Zangari M; Yoon D; Yu SM Visualizing collagen proteolysis by peptide hybridization: From 3D cell culture to in vivo imaging. Biomaterials 2018, 183, 67–76. [PubMed: 30149231]

(28). Barth D; Milbradt AG; Renner C; Moroder LA (4*R*)- or a (4*S*)-fluoroproline residue in position Xaa of the (Xaa-Yaa-Gly) collagen repeat severely affects triple-helix formation. ChemBioChem 2004, 5, 79–86. [PubMed: 14695516]

(29). Hodges JA; Raines RT Stereoelectronic and steric effects in the collagen triple helix: Toward a code for strand association. J. Am. Chem. Soc 2005, 127, 15923–15932. [PubMed: 16277536]

(30). Shoulders MD; Guzei IA; Raines RT 4-Chloroprolines: Synthesis, conformational analysis, and effect on the collagen triple helix. Biopolymers 2008, 89, 443–454. [PubMed: 17937398]

(31). Bretscher LE; Jenkins CL; Taylor KM; DeRider ML; Raines RT Conformational stability of collagen relies of a stereoelectronic effect. J. Am. Chem. Soc 2001, 123, 777–778. [PubMed: 11456609]

(32). Hodges JA; Raines RT Stereoelectronic effects on collagen stability: The dichotomy of 4-fluoroproline diastereomers. J. Am. Chem. Soc 2003, 125, 9262–9263. [PubMed: 12889933]

(33). Wadas TJ; Wong EH; Weisman GR; Anderson CJ Coordinating radiometals of copper, gallium, indium, yttrium, and zirconium for PET and SPECT imaging of disease. Chem. Rev 2010, 110, 2858–2902. [PubMed: 20415480]

(34). Tsionou MI; Knapp CE; Foley CA; Munteanu CR; Cakebread A; Imberti C; Eykyn TR; Young JD; Paterson BM; Blower PJ; Ma MT Comparison of macrocyclic and acyclic chelators for gallium-68 radiolabelling. RSC Adv. 2017, 7, 49586–49599. [PubMed: 29308192]

(35). Afshar-Oromieh A; Hetzheim H; Kratochwil C; Benesova M; Eder M; Neels OC; Eisenhut M; Kübler W; Holland-Letz T; Giesel FL; Mier W; Kopka K; Haberkorn U The theranostic PSMA ligand PSMA-617 in the diagnosis of prostate cancer by PET/CT: Biodistribution in humans, radiation dosimetry, and first evaluation of tumor lesions. J. Nucl. Med 2015, 56, 1697–1705. [PubMed: 26294298]

(36). Hambidge M Human zinc deficiency. J. Nutr 2000, 130 (5), 1344S–1349S. [PubMed: 10801941]

(37). Hennrich U; Benešová M [^{68}Ga]Ga-DOTA-TOC: The first FDA-approved ^{68}Ga-radiopharmaceutical for PET imaging. Pharmaceuticals 2020, 13, 38. [PubMed: 32138377]

(38). Hennrich U; Eder M [^{68}Ga]Ga-PSMA-11: The first FDA-approved ^{68}Ga-radiopharmaceutical for PET imaging of prostate cancer. Pharmaceuticals 2021, 14, 713. [PubMed: 34451810]

(39). Mueller D; Breeman WAP; Klette I; Gottschaldt M; Odparlik A; Baehre M; Tworowska I; Schultz MK Radiolabeling of DOTA-like conjugated peptides with generator-produced ^{68}Ga and using NaCl-based cationic elution method. Nat. Protoc 2016, 11, 1057–1066. [PubMed: 27172166]

(40). Bennink LL; Smith DJ; Foss CA; Pomper MG; Li Y; Yu SM High serum stability of collagen hybridizing peptides and their fluorophore conjugates. Mol. Pharmaceutics 2017, 14, 1906–1915.

(41). Walters DM; Kleeberger SR Mouse models of bleomycin-induced pulmonary fibrosis. Curr. Protoc. Pharmacol 2008, 40, 5.46.1–5.46.17.

(42). Moeller A; Ask K; Warburton D; Gauldie J; Kolb M The bleomycin animal model: A useful tool to investigate treatment options for idiopathic pulmonary fibrosis? Int. J. Biochem. Cell Biol 2008, 40 (1), 362–382. [PubMed: 17936056]

(43). Gorres KL; Raines RT Prolyl 4-hydroxylase. Crit. Rev. Biochem. Mol 2010, 45, 106–124.

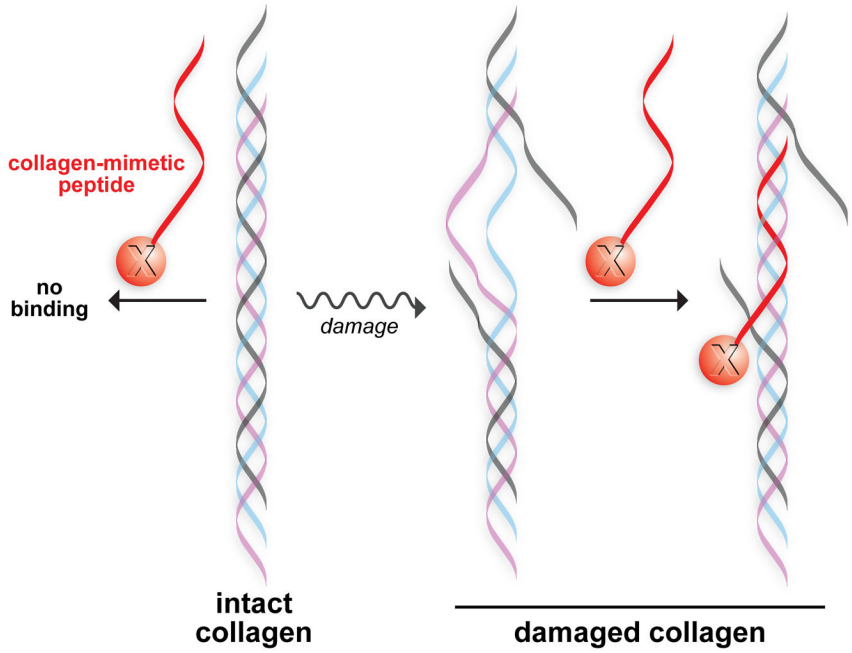

Figure 1.

Conceptual representation of a collagen-mimetic peptide annealed to a damaged collagen triple helix. A pendant moiety, “X”, becomes anchored in the damaged collagen.

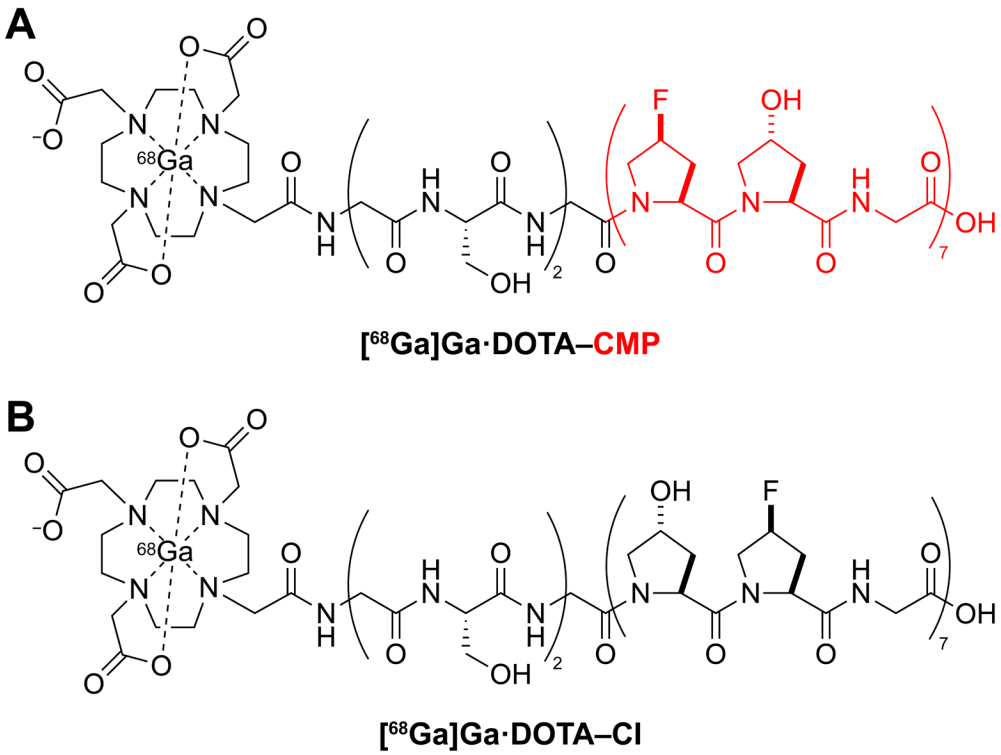

Figure 2.

(a) Structure of [^{68}Ga]Ga·DOTA–CMP. The CMP segment is depicted as a red ribbon in Figure 1. (b) Structure of [^{68}Ga]Ga·DOTA–CI.

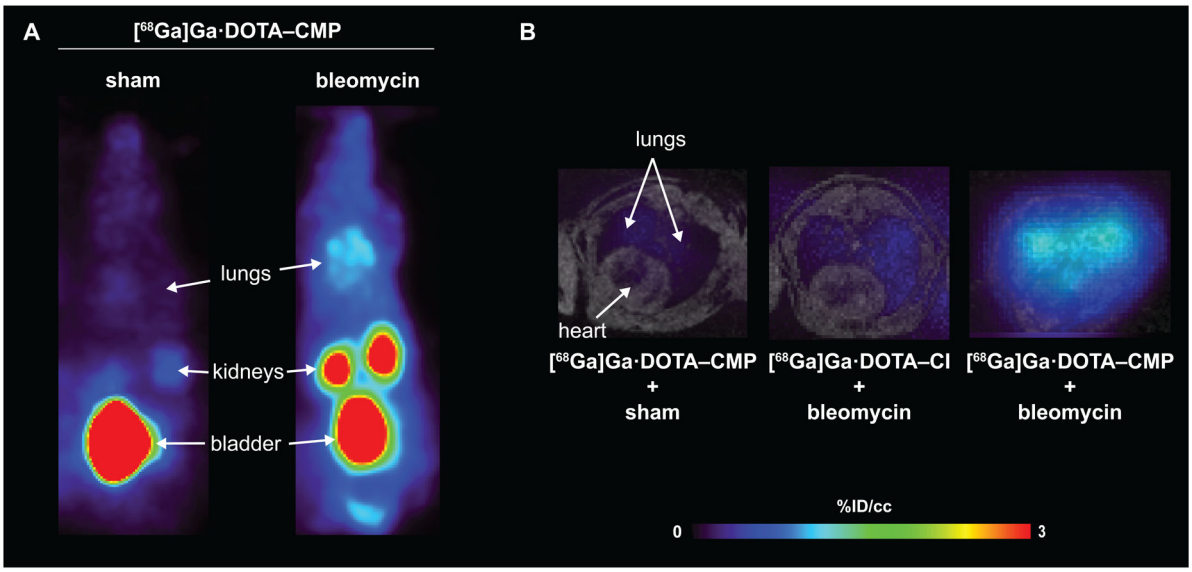

Figure 3.

PET and fused PET–MR images of sham and bleomycin-injured mice 50–60 min after tail-vein injection with [^{68}Ga]Ga·DOTA–CMP or [^{68}Ga]Ga·DOTA–CI (A) Representative coronal maximum-in-projection (MIP). (B) Representative axial fused PET (color scale) – MR (gray scale) images of the lungs and heart.

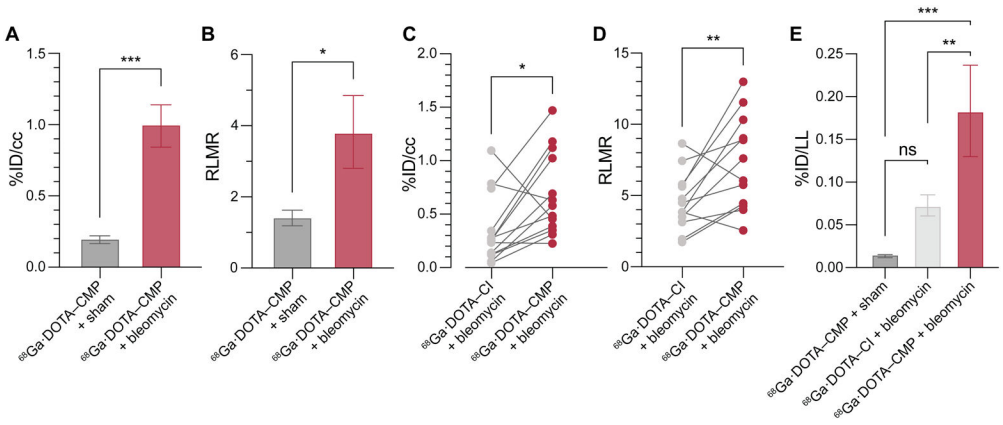

Figure 4.

Radiation signal in organs from sham and bleomycin-injured mice injected with [^{68}Ga]Ga·DOTA–CMP or [^{68}Ga]Ga·DOTA–CI. (A) In vivo %ID/cc values in right lungs 50–60 min post-injection as measured by PET. (B) In vivo right lung:muscle ratios (RLMRs) 50–60 min post-injection as measured by PET. In panels A and B, $n = 6$ for [^{68}Ga]Ga·DOTA–CMP + sham and $n = 5$ for [^{68}Ga]Ga·DOTA–CMP + bleomycin. (C) and (D) show data from a paired study, in which mice were injected with [^{68}Ga]Ga·DOTA–CMP and imaged, then 24 h later, injected with [^{68}Ga]Ga·DOTA–CI and imaged. (C) In vivo %ID/cc values in right lungs 50–60 min post-injection as measured by PET. Connecting lines indicate associated data points from individual animals. (D) In vivo RLMRs 50–60 min post-injection as measured by PET. Connecting lines indicate associated data points from individual animals. (E) Ex vivo %ID/lung left uptake 90 min post-injection. In panel E, $n = 6$ for [^{68}Ga]Ga·DOTA–CMP + sham, $n = 13$ for [^{68}Ga]Ga·DOTA–CI + bleomycin, and $n = 5$ for [^{68}Ga]Ga·DOTA–CMP + bleomycin. An unpaired *t*-test was performed on the data in panels A and B. A paired *t*-test was performed on the data in panels C and D. A one-way ANOVA with a post-hoc Tukey test was performed on the data in panel E. Values are the mean ± SE. *$P < 0.05$, **$P < 0.01$, ***$P < 0.001$.